Applied Radiation and Isotopes 140 (2018) 41–49

Contents lists available at ScienceDirect

Applied Radiation and Isotopes

journal homepage: www.elsevier.com/locate/apradiso

Self-adaption Compton imaging algorithm for a quasi-point source

Guo Xiaofeng[a,b], Xiang Qingpei[a,*], Tian Dongfeng[a], Hao Fanhua[a], Wang Yi[b], Zhang Yingzeng[a]

[a] Institute of Nuclear Physics and Chemistry, China Academy of Engineering Physics, Mianyang 621900, China
[b] Department of Engineering Physics, Tsinghua University, Beijing 100084, China

ARTICLE INFO

Keywords:
Compton imaging
Self-adaption
Backward-scattering
Monte Carlo simulation

ABSTRACT

Compton imaging is a promising technology for various applications including nuclear safety, nuclear medicine, and astrophysics. For quasi-point-source applications, which are widely found in practice, a novel Compton imaging algorithm incorporating the concept of self-adaption is proposed that provides excellent precision and high efficiency. In particular, this algorithm significantly improves the imaging precision of backward-scattering imaging events so that they can be revived for reconstruction without degrading image quality. From Monte Carlo simulations, a comparison between the self-adaption Compton imaging algorithm and the conventional Compton imaging algorithm was conducted, and the feasibility and reliability of this algorithm was verified in various scenarios.

1. Introduction

Since the 1970s, when the concept of Compton imaging was first proposed (Schonfelder et al., 1973; Todd et al., 1974), continual developments have been made over nearly 50 years. In the past 20 years, in particular, the development of electronics and detectors has produced rapid advances in the Compton imager. To improve imaging efficiency and precision, many advanced systems and algorithms have been proposed. For example, a system structure of the original prototype Compton imager, consisting of a scattering detector and an absorbing detector (HPGe/HPGe) (Haskins et al., 1996), was developed into a portable 4π-direction- sensitive Compton imager using a single CdZnTe detector (3D-CZT) (Du et al., 2007), as well as a multi-mode structure that incorporated a coded aperture (MURA + CsI/CsI) (Lee and Lee, 2014). An imaging algorithm also was developed to perform filtered back projection (FBP) rather than simple back projection (SBP) (Xu and He, 2006), and maximum likelihood expectation maximization (MLEM) (Du et al., 2007; Dempster et al., 1977; Kim et al., 2017). Furthermore, with the development of low-noise electronic readout circuits (Tajima et al., 2004) and the advent of three-dimensional imaging for extended sources (Kishimoto et al., 2015; Domingo-Pardo, 2012), more researchers were focusing on practical application of the Compton imager.

Basically, regardless of system structure and imaging algorithm, there are always two types of imaging events in a Compton imager, namely, forward-scattering imaging events (FSIEs) and backward-scattering imaging events (BSIEs). Because of the short time interval (< 1 ns) between scattering and absorption interactions, the detection system finds it nearly impossible to distinguish their order, so that all imaging events can only be considered as desired FSIEs, which leads to miss-reconstructions of BSIEs. As a result, the imaging background increases and the imaging precision degrades. We call this phenomenon the 'backward-scattering effect' (BSE).

In our previous work (Guo et al., 2017), a Compton imager consisting of double-layered CZT pixel-array detectors was proposed that had great efficiency and precision. Studies show that there are a large number of BSIEs generated in Compton imagers with high-Z materials as front detectors (or both front and back detectors if using the same material), but the imaging precision of BSIEs is much worse than that of FSIEs. Unfortunately, these BSIEs have to be discarded to guarantee the imaging precision of a Compton imager.

Many researchers are aware of the BSE, but there are few reports regarding reviving BSIEs. The research mainly focuses on eliminating BSIEs or attenuating BSE, such as backscatter-rejection using energy thresholds (Saull et al., 2012) and Compton kinematic discrimination (Boggs and Jean, 2000), as well as artifact-reduction using MLEM (Du et al., 2007). Indeed, these methods improve imaging precision and signal-to-noise ratio (SNR), but discarding a large number of BSIEs is a great loss. Given that the imaging efficiency of the Compton imager is extremely low, improving the imaging precision of BSIEs would be significant so that they can be revived and used in image reconstruction.

To this end, we have proposed an approach called the 'self-adaption Compton imaging algorithm' (SCIA). This algorithm can significantly improve the imaging precision of BSIEs and also the effectiveness for FSIEs. It has wide applications for quasi-point-source imaging, such as

* Corresponding author.
E-mail address: xiangqingpei@163.com (X. Qingpei).

https://doi.org/10.1016/j.apradiso.2018.06.006
Received 27 February 2018; Received in revised form 26 May 2018; Accepted 5 June 2018
Available online 07 June 2018
0969-8043/

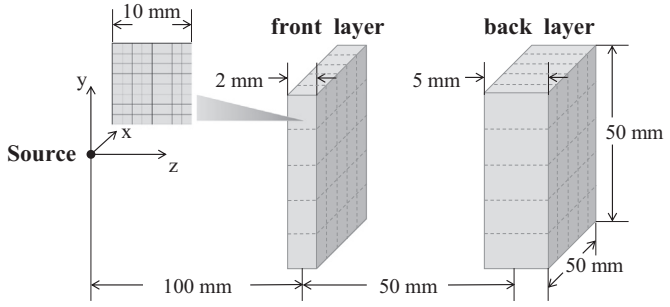

Fig. 1. System structure of the Compton imager based on double-layered CZT pixel-array detectors.

source localization over a long distance in nuclear safety, lesion imaging in nuclear medicine, and astronomical observations in astrophysics. In this paper, the validity and feasibility of SCIA is fully demonstrated using Monte Carlo simulations, performed on the Geant4 10.0 platform with the default standard EM physics employed (based on the basic example B2a).

2. Algorithm

2.1. System modeling

The Compton imager consists of double-layered CZT pixel-array detectors (Guo et al., 2017) (Fig. 1). Both front and back layers consist of 5 × 5 CZT detectors, with each detector having size 10 × 10 mm^2 divided into 8 × 8 pixels. The thickness of the front and back layers are 2 mm and 5 mm, respectively, and hence, the overall layer dimensions are 2 × 50 × 50 mm^3 and 5 × 50 × 50 mm^3, respectively. The distance between the two layers is 50 mm, and the distance between the source plane and the front layer is 100 mm.

During the analysis and processing of imaging data, we fully considered the energy and position resolutions of the detectors. The experimental results show that the energy resolution is about 5.13% @ 59.5 keV (^{241}Am) and 1.64% @ 662 keV (^{137}Cs). Depending on the anode-pixel segmentation and the depth-sensing technology of the CZT detectors, the position resolution of the X and Y directions is set to 1.25 mm, whereas that of the Z direction is set to 0.5 mm (Guo et al., 2017).

For convenience and effectiveness of study, a true point source was employed using particle gun in Geant4 to evaluate the best performance of SCIA to the theoretical limits. However, in the actual application scenario, there is no true point source. Actually, for a real source distributed over a certain area or volume, if it is much smaller than the detectors, or it is located far away from the detectors so that the distributed size can be negligible to the distance, then this source can be taken as a "quasi-point source". Basically, the imaging results of a quasi-point source should be very close to that of a true point source, with only a little dispersion or broadening.

If not special stated in the following text, the source is set to be a ^{137}Cs point source at the center (x, y, z) = (0, 0, 0) [mm], with 2.9 × 10^7 particles emitted toward the front layer simulated (i.e. the emitting range is a cone edged by four vertices on the front surface of the front detector). According to the system structure, it is equivalent to nearly 10^9 particles emitted form a 4π isotropic source, and there are almost 1.85 × 10^7 events entered the sensitive area of detectors.

2.2. Events selection

Based on the Compton-imaging principle, we specify the imaging-event selection criteria as (Guo et al., 2017): (1) Both front and back layers register energy depositions simultaneously ($E_1 > 0$ and $E_2 > 0$); (2) Total energy ($E_1 + E_2$) must be within the full energy peak ($E_0 \pm 3\sigma$); (3) Energy deposition must occur only in a single pixel for both layers. Only events meeting these three criteria are used in image reconstructions.

As a result, there are 16,746 imaging events matching these criteria, which is nearly 0.09% relative to all the events entered the sensitive area of detectors. Among them, there are three types of imaging events screened out: (1) Events scattered in the front layer and absorbed in the back layer, as FSIEs; (2) Events scattered in the back layer and absorbed in the front layer, as BSIEs; (3) Other undesirable events include, but not limited to, events tagged as false imaging events (FIEs), where a source photon occurs from the photo-electric effect in one layer, and a photoelectron escapes or produces a bremsstrahlung photon, which is then absorbed in the other layer.

For the Compton imager based on double-layered CZT pixel-array detectors, the simulation results show that the number of FSIEs and BSIEs is almost the same, whereas FIEs account for only a small proportion. FSIEs and BSIEs dominate imaging events, but they cannot be distinguished by the interaction sequence because the imaging system has a limited time resolution. Fortunately, in energy depositions, BSIEs have a concentrated distribution, which can be used as a criterion for the discrimination of FSIEs and BSIEs. For example, for the ^{137}Cs (662 keV) point source placed on the central axis of the two layers, the energy deposition of FSIEs is widely distributed over 0–300 keV in the front layer and 360–670 keV in the back layer, whereas the energy deposition of BSIEs is concentrated in 180–200 keV in the front layer and 460–485 keV in the back layer, which implies there are only 5.8% FSIEs within this range. In the actual application scenario, all the imaging events matching the above criteria can be classified approximately as FSIEs and BSIEs using the energy threshold method. As a result, the number of FSIEs and BSIEs are 8723 and 8023, respectively. In order to demonstrate the entire process of SCIA and to exclude interference from difference between event data groups, these events data above are used as a default example for the imaging results from Section 2.3 to Section 4.2.

2.3. Basis of SCIA

For a typical Compton imaging event [Fig. 2(b)], the source photon scatters in one layer with a corresponding energy deposition E_e and scattering position C, and is then absorbed in the other layer with corresponding energy deposition E_γ and absorption position A. The conventional SBP algorithm is described as follows: First, the Compton scattering angle (θ_C) is calculated by substituting E_e and E_γ into the Compton scattering formula

$$\cos\theta_C = 1 - \frac{m_0c^2 \cdot E_e}{(E_e + E_\gamma)\cdot E_\gamma} \tag{1}$$

where θ_C is the Compton scattering angle, m_0c^2 = 511 keV the rest energy of the electron, E_e and E_γ are the energies of the recoil electron and scattered photon, respectively. Second, the source is located on the surface of a back-projected cone, for which the axis is AC and the half-angle is θ_C. Finally, the source location should be the intersection of multi-cones projected by all the imaging events.

However, the energy resolution of detectors causes measurement errors in E_e and E_γ, which results in an uncertainty in θ_C. Therefore, the cones reconstructed with θ_C may not always pass through the true source location. Hence the intersection of the multi-cones will be a source image with some artifacts [pink thick lines in Fig. 2(b)].

At the same time, if a reference point (P) is arbitrarily ascribed on the source plane, a geometric angle (θ_{geom}) can be formed by the three points (P, C and A),

$$\cos\theta_{geom} = \frac{\overrightarrow{PC}\cdot\overrightarrow{CA}}{|\overrightarrow{PC}|\cdot|\overrightarrow{CA}|} \tag{2}$$

where θ_{geom} is the geometric angle, P the reference point, C and A are